Electron-impact study of the SO radical using the *R*-matrix method

Jasmeet Singh Rajvanshi* and K. L. Baluja†
Department of Physics and Astrophysics, University of Delhi, Delhi 110007, India
(Received 28 April 2010; published 15 September 2010)

The SO radical with an even number of electrons belongs to an open-shell system due to its π^2 ground-state electronic configuration. This configuration gives rise to three low-lying states $X\,^3\Sigma^-$, $a\,^1\Delta$, and $b\,^1\Sigma^+$. The inclusion of these target states in a trial wave function of the entire scattering have important implications in the resonances that may be detected in this open-shell molecule. The *R*-matrix method is a well-established *ab initio* formalism which is employed to calculate elastic differential and integral cross sections, momentum-transfer cross sections, and inelastic cross sections. The Hartree-Fock ground-state configuration of SO is $1\sigma^2 2\sigma^2 3\sigma^2 4\sigma^2 1\pi^4 5\sigma^2 6\sigma^2 7\sigma^2 2\pi^4 3\pi^2$. We have included 28 target states in the trial wave function of the scattering system. In our configuration-interaction (CI) model, we freeze 12 electrons in orbitals 1σ, 2σ, 3σ, 4σ, and 1π, the remaining 12 electrons are free to move among the eight orbitals 4σ, 5σ, 6σ, 7σ, 8σ, 9σ, 2π, and 3π. We have carried our scattering calculations in static-exchange, one-state with CI wave function, and 28-state models. We have detected a stable anionic bound state $^2B_1$ of SO at various bond lengths of SO molecule. The vertical electron affinity value is 0.970 eV, which is comparable to the experimental value of 1.125 eV. We also detected two core-excited shape resonances, both of $^2\Pi$ symmetry and with $^1\Delta$ and $^1\Sigma^+$ as the parent states.

DOI: 10.1103/PhysRevA.82.032706 PACS number(s): 34.80.Bm, 34.80.Gs, 34.80.Ht

I. INTRODUCTION

Sulfur-containing compounds are important in many processes. It is well known that SO_2 is one of the major atmospheric pollutants to cause acid rain. During the eruption of volcanoes or the use of fossil fuels, a large amount of this gas is thrown into the Earth's atmosphere. The SO_2-containing plasmas also play an important role in planetary atmospheres [1,2]. The low-temperature processing plasmas containing SO_2 have been employed in the plasma-assisted surface treatment of biocompatible material and biomedical devices [3], the SO radical is an abundant byproduct of the plasma remediation of SO_2 from any combustion source using fossil fuels [4,5]. Sulfur oxide is a species of both astrochemical [6] and technological importance [7]. Technologically, it is used as a laser in the near-ultraviolet region. At the molecular level, the $a\,^3\Pi$–$X\,^3\Sigma^-$ transition is the one involved in the lasing process in SO. In the literature, the determination of partial and total ionization cross sections have been reported [8]. Recently, a study on electron collision with SO and some other sulfur-containing molecules using a spherical complex potential was reported [9], and in that study, elastic integral and grand-total cross sections and total ionization cross sections for incident energies ranging from ionization threshold to 2000 eV were computed. In the theoretical area, a very recent calculation was performed at the static-exchange-polarization-absorption level of approximation using a combination of the iterative Schwinger variation method [10] and the distorted-wave approximation. More specifically, in that study, differential cross sections (DCSs), integral cross sections (ICSs), and momentum-transfer cross sections (MTCSs) were computed in the 1–500 eV energy range.

The present study applies the *ab initio* *R*-matrix method to low-energy scattering of the SO molecule in the fixed nuclei approximation. The calculations use code developed by the UK Molecular *R*-Matrix Group [11,12]. The *R*-matrix method has the advantage over other scattering methods in efficiently providing cross sections at a large number of scattering energies. It also has the ability to include correlation effects and give an adequate representation of several excited states of the molecule [13]. We are interested in the low-energy region ($\leqslant$10 eV) which is a favorite ground for the *R*-matrix method. The incoming electron can occupy one of the many unoccupied molecular orbitals or can excite any of the occupied molecular orbital as it falls into another one. These processes give rise to the phenomenon of resonances forming a negative molecular ion for a finite time before the resonance decays into energetically open channels.

Electron scattering calculations are performed at static exchange, one-state CI and close-coupling approximation in which we have retained 28 target states in the *R*-matrix formalism. The integrated elastic, differential, and momentum cross sections for electron impact on the SO molecule from its ground state are reported. The excitation cross sections from the ground state to few low-lying excited states have also been calculated. We have also computed the binary-encounter-Bethe (BEB) ionization cross section [14,15]. The BEB cross sections depend only on the binding energies, kinetic energies, and the occupation number of the occupied molecular orbitals of the target and on the energy of the incident electron. The momentum-transfer cross sections calculated in the *R*-matrix approximation have been used to calculate effective collision frequency over a wide electron temperature range. We must point out that the *R*-matrix approach is not the only scattering method that allows the *ab initio* inclusion of correlation effects and is applicable to studies of open-shell targets. The complex Kohn variational method has been successfully employed for polyatomic targets [16].

*Also at Keshav Mahavidyalaya, Physics and Electronics Department, University of Delhi; rajvanshi_jasmeet@yahoo.co.in
†kl_baluja@yahoo.com

II. METHOD

A. Theory

In an R-matrix approach [17,18], the configuration space of the scattering system is divided into two spatial regions: an inner region and an outer region. These regions are treated differently in accordance with the different interactions in each region. The center of the R-matrix sphere coincides with the center of mass of the molecule. When the scattering electron leaves the inner region, the other target electrons are confined to the inner region. In the present work, the R-matrix boundary radius dividing the two regions was chosen to be $10a_0$, centered at the SO center of mass. This sphere encloses the entire charge cloud of the occupied and virtual molecular orbitals included in the calculation. At $10a_0$, the amplitudes of the molecular orbitals are less than $10^{-5}a_0^{-3/2}$. However, the continuum orbitals have finite amplitudes at the boundary. Inside the R-matrix sphere, the electron-electron correlation and exchange interactions are strong. Short-range correlation effects are important for accurate prediction of large-angle elastic scattering, and exchange effects are important for spin-forbidden excitation cross sections. A multicentered CI wave-function expansion is used in the inner region. The calculation in the inner region is similar to a bound-state calculation, which involves the solution of an eigenvalue problem for $(N+1)$ electrons in the truncated space, where there are N target electrons and a single scattering electron. Most of the physics of the scattering problem is contained in this $(N+1)$ electron bound-state molecular-structure calculation. Outside the sphere, only long-range multipolar interactions between the scattering electron and the various target states are included. Because only direct potentials are involved in the outer region, a single center approach is used to describe the scattering electron via a set of coupled differential equations. The R matrix is a mathematical entity that connects the two regions. It describes how the scattering electron enters and leaves the inner region. In the outer region, the R matrix on the boundary is propagated outward [19,20] until the inner-region solutions can be matched with asymptotic solutions, thus yielding the physical observables such as cross sections. We include only the dipole and quadrupole moments in the outer region.

In the polyatomic implementation of the UK molecular R-matrix code [11,12], the continuum molecular orbitals are constructed from atomic Gaussian-type orbitals (GTOs) using basis functions centered on the center of gravity of the molecule. The main advantage of GTOs is that integrals involving them over all space can be evaluated analytically in closed form. However, a tail contribution is subtracted to yield the required integrals in the truncated space defined by the inner region [11].

The target molecular orbital space is divided into core (inactive), valence (active), and virtual orbitals. The target molecular orbitals are supplemented with a set of continuum orbitals, centered on the center of gravity of the molecule. The continuum basis functions used in polyatomic R-matrix calculations are Gaussian functions and do not require fixed boundary conditions. First, target and continuum molecular orbitals are orthogonalized using Schmidt orthogonalization. Then symmetric or Löwdin orthogonalization is used to orthogonalize the continuum molecular orbitals among themselves and remove linearly dependent functions [11,21]. In general and in this work, all calculations are performed within the fixed-nuclei approximation. This is based on the assumption that electronic, vibrational, and rotational motions are uncoupled.

In the inner region, the wave function of the scattering system, consisting of target plus scattering electron, is written using the CI expression

$$\Psi_k^{N+1} = A\sum_i \phi_i^N(x_1,\ldots,x_N)\sum_j \xi_j(x_{N+1})a_{ijk} + \sum_m \chi_m(x_1,\ldots,x_N,x_{N+1})b_{mk}, \quad (1)$$

where A is an antisymmetrization operator, x_N is the spatial and spin coordinates of the Nth electron, ϕ_i^N represents the ith state of the N-electron target, ξ_j is a continuum orbital spin-coupled with the scattering electron, and k refers to a particular R-matrix basis function. Coefficients a_{ijk} and b_{mk} are variational parameters determined as a result of the matrix diagonalization. To obtain reliable results, it is important to maintain a balance between the N-electron target representation, ϕ_i^N, and the $(N+1)$ electron-scattering wave function. The summation in the second term of Eq. (1) runs over configurations χ_m, where all electrons are placed in target-occupied and virtual molecular orbitals. The choice of appropriate χ_m is crucial in this [22]. These are known as L^2 configurations and are needed to account for orthogonality relaxation and for correlation effects arising from virtual excitation to higher electronic states that are excluded in the first expansion. The basis for the continuum electron is parametrically dependent on the R-matrix radius and provides a good approximation to an equivalent basis of orthonormal spherical Bessel functions [23]. In the one-state CI model, we have included ground state only but have used a CI wave function to describe it. In the 28-state model calculation, each target state is represented by a CI wave function.

B. SO target model

The molecule SO is a linear open-shell system that has ground state $X\,^3\Sigma^-$ in the $C_{\infty v}$ point group which is reduced to the C_{2v} point group when the symmetry is lowered. In the R-matrix suite of programs, the highest Abelian group is D_{2h}, and therefore we work in the C_{2v} point group, which is a subset of the D_{2h} point group. The results are reported in the natural symmetry point group as well as in the C_{2v} point group for the sake of convenience. We used a double zeta plus polarization (DZ + P) Gaussian basis set [24] contracted as (12,8,1)/(6,4,1) for S and (9,5,1)/(4,2,1) for O. We avoided using diffuse functions, as these would extend outside the R-matrix box. We first performed a self-consistent-field (SCF) calculation for the ground state of the SO molecule with the chosen DZP basis set and obtained a set of occupied orbitals and a virtual set of orbitals.

The Hartree-Fock electronic configuration for the ground state is $1\sigma^2 2\sigma^2 3\sigma^2 4\sigma^2 1\pi^4 5\sigma^2 6\sigma^2 7\sigma^2 2\pi^4 3\pi^2$ that gives rise to lowest-lying $X\,^3\Sigma^-$, $a\,^1\Delta$, and $b\,^1\Sigma^+$ states correlating with the first dissociation channel $[S(^3P) + O(^3P)]$. The energy of the occupied 3π orbital is -11.12 eV, and by

TABLE I. Properties of the SO target, ground-state energy, and dipole moment (in a.u.) and the ionization potential (IP, in eV), SCF at bond length $R_e = 2.777a_0$, and CI at bond length $R_e = 2.9a_0$.

	Present work		Previous theory			
	SCF	CI	SCF[a]	CI[a]	CSP-ic[b]	ISVM DWA[c]
E	−472.333 53	−472.380 80	−472.333 54	−472.511 70		−472.137 52
μ	0.96	0.79	0.95	0.77	0.61	0.73
IP	11.12	11.12			10.29	

[a]W. C. Swope *et al.* [26].
[b]Joshipura and Gangopadhyay [9].
[c]Lee *et al.* [10].

Koopman's theorem it is the first ionization energy. Since the SCF procedure is inadequate to provide a good representation of the target states, we improve the energy of the ground as well as the excited states by using CI wave functions. This lowers the energies, and the correlation introduced provides a better description of the target wave function and excitation energies. In our limited CI model, we keep 12 electrons frozen in the $1\sigma^2 2\sigma^2 3\sigma^2 4\sigma^2 1\pi^4$ configuration and allow the remaining 12 electrons to move freely in molecular orbitals 4σ, 5σ, 6σ, 7σ, 8σ, 9σ, 2π, and 3π. The CI ground-state energy for the SO molecule is −472.3808 hartrees, at a bond length of $R_e = 2.9a_0$. We computed the value of vertical electronic affinity (VEA) by performing a bound-state calculation of SO^- by including the continuum electron basis functions centered at the origin. The VEA is equal to the difference between the total energy of the neutral molecule and its anion at the equilibrium geometry of the neutral molecule. We detect a stable bound state of SO^- with $^2\Pi$ symmetry having the configuration $1\sigma^2 2\sigma^2 3\sigma^2 4\sigma^2 1\pi^4 5\sigma^2 6\sigma^2 7\sigma^2 2\pi^4 3\pi^3$ with a VEA of 0.970 eV, which is in good agreement with the estimated experimental (adiabatic) value of about 1.125 eV [25].

To provide additional information on the charge distribution in the SO molecule, we have also calculated the dipole and quadrupole moments. In our CI model the dipole moment and the absolute values of the quadrupole component Q_{20} for the ground state are 0.7945 and 0.86 a.u., respectively. The values of the ground-state energy, dipole moment, and the ionization potential are compared with other work in Table I.

In Table II, we list the dominant configuration, the transition moments, number N of configuration state functions (CSFs), dipole moments, and vertical excitation energies (VEEs) for the target states. We have good agreement with the calculation of Borin *et al.* [27] for VEEs and dipole and transition moments, who employed a state-averaged complete active space self-consistent field, internally contracted multireference configuration interaction approach using quintuple-zeta basis sets.

C. Scattering model

We have included 28 target states (three of $^1A_2$, four of $^3A_2$, four of $^1A_1$, two of $^3A_1$, three of $^1B_1$, five of $^3B_1$, three of $^1B_2$, and five of $^3B_2$) in the trial wave function describing the electron plus target system. However, excitation cross sections are reported only for the four excited states ($a\,^1\Delta$, $b\,^1\Sigma^+$, $B\,^3\Sigma^-$, and $C\,^3\Pi$) that lie below the first ionization threshold. Calculations were performed for doublet and quartet scattering states with A_1, A_2, B_1, and B_2 symmetries. Continuum orbitals up to $l = 4$ (g-partial wave) were included in the scattering calculation. Due to the presence of the long-range dipole interaction, the elastic cross sections are formally divergent in the fixed-nuclei approximation, because the differential cross section is singular in the forward direction. To obtain converged

TABLE II. Dominant configuration, transition moments (in a.u.), number N of configuration state functions (CSFs), the vertical excitation energies (VEEs in eV), and dipole moments (μ in a.u.) for the target states of SO at bond length $R_e = 2.9a_0$.

State	VEE (eV)		Transition		μ (a.u.)	
$C_{2v}/C_{\infty v}$	Present	Previous[a]	moments (a.u.)	N	Present	Previous[a]
$X\,^3A_2/X\,^3\Sigma^-$	0.0	–	–	864	0.79	0.62
$a(^1A_2,^1A_1)/a\,^1\Delta$	0.75	0.71	–	584 696	0.73	0.59
$b(^1A_1)/b\,^1\Sigma^+$	1.14	1.28	–	696	0.71	0.55
$c(^1A_2)/c\,^1\Sigma^-$	3.95	4.20	–	584	0.04	0.03
$A'(^3A_2,^3A_1)/A'\,^3\Delta$	4.10	4.40	0.002	864 822	0.04	0.07
$A''(^3A_1)/A''\,^3\Sigma^+$	4.21	4.50	–	822	0.04	0.06
$A\,^3B_1,^3B_2/A\,^3\Pi$	5.53	4.92	0.013	858	0.38	0.25
$C\,^3B_1,^3B_2/C\,^3\Pi$	5.84	5.70	0.173	858	0.37	0.26
$d\,^1B_2,^1B_1/d\,^1\Pi$	6.62	5.62	–	620	0.36	0.18
$e\,^1B_2,^1B_1/e\,^1\Pi$	6.71	6.65	–	620	0.33	0.21
$B\,^3A_2/B\,^3\Sigma^-$	7.06	5.90	0.645	864	0.22	0.28

[a]Borin *et al.* [27].

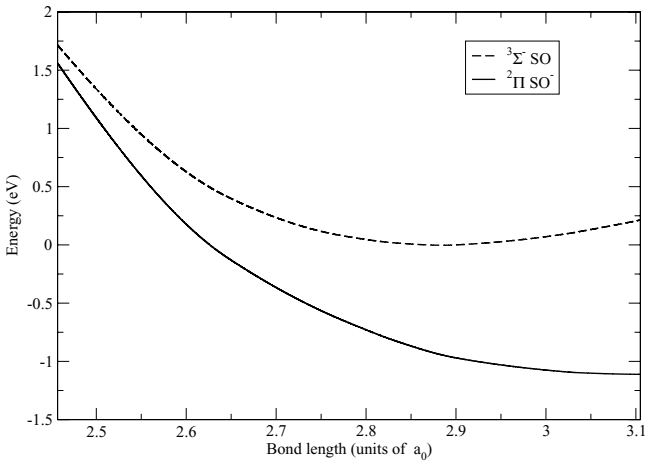

FIG. 1. Ground-state potential energy curves of SO and SO^- molecules. Dashed curve, SO; solid curve, SO^-.

cross sections, the effect of rotation must be included along with a very large number of partial waves. The effects of partial waves with $l > 4$ were included using a Born correction via a closure approach [28]. Our g-partial wave cross section using the R-matrix method nearly coincided with the g-wave Born results. This establishes the correctness of our procedure to use Born correction beyond the g-partial wave. The use of the rotationally resolved Born closure procedure has also been put forth in [29].

III. RESULTS

A. Elastic and inelastic total cross sections

The ground-state electronic configuration of SO has two unpaired π electrons. Due to vacancy in the 3π orbital of the ground state of SO, the scattering electron can occupy it, forming a stable anionic ground state of SO with symmetry $^2\Pi$. In our 28-state model, we found an R-matrix pole at -472.4164 a.u. at R_e in the scattering symmetry $^2\Pi$ which is lower than the energy -472.3808 a.u. of ground state $X\,^3\Sigma^-$

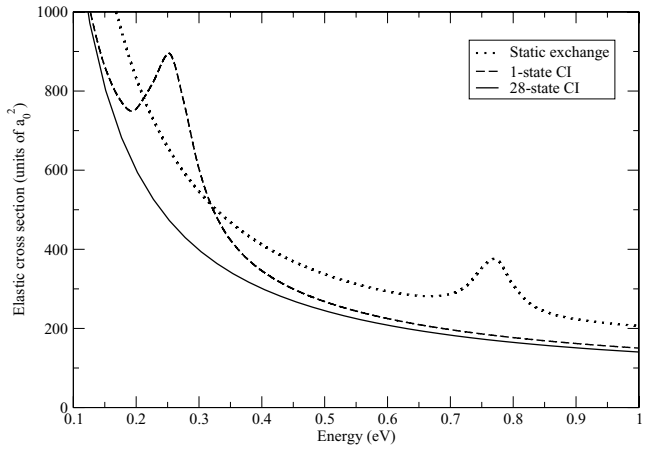

FIG. 2. Elastic cross sections of the electron impact on the SO molecule. Dotted curve, SCF at a bond length $R_e = 2.777a_0$; dashed curve, one-state CI, and solid curve, 28-state CI calculations at a bond length $R_e = 2.9a_0$.

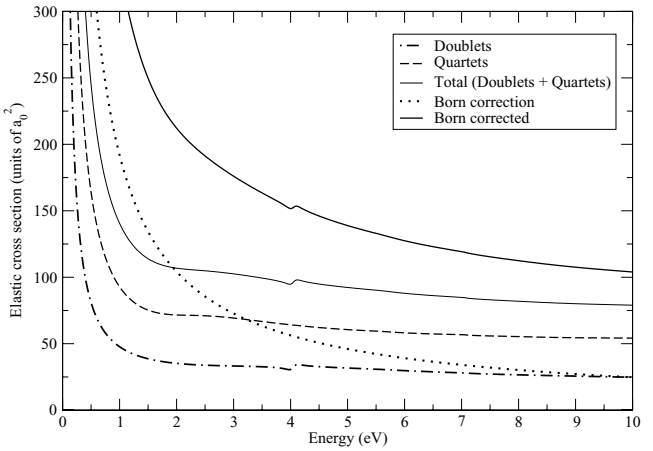

FIG. 3. Elastic cross sections of the electron impact on the SO molecule at R_e for 28-state calculations. Dash-dot curve, doublets sum ; dashed curve, quartets sum; thin solid curve, total (doublets + quartets); dotted curve, Born correction; thick solid line, Born corrected (sum of doublets, quartets, and Born correction).

of SO, which indicates the detection of an anionic bound state. We calculated the bound-state energies of this anionic $^2\Pi$ state at different bond length by performing an L^2-type calculation. The potential-energy curves of the $^3\Sigma^-$ state of the SO molecule and $^2\Pi$ state of the SO^- anion are shown in Fig. 1. The anion is stable at all the bond lengths. This yields a vertical electron affinity of 0.97 eV at R_e. From Fig. 1, we find that the equilibrium bond length for the ground state of the anion SO^- is $3.1a_0$. The S–O bond length is about 6.9% elongated in the anionic state SO^- because the extra electron is in a Π^* orbital. Our value of electron affinity is 0.970 eV, which is in good agreement with the estimated experimental (adiabatic) value of about 1.125 eV [25].

In Fig. 2, we have summed the contribution of doublet and quartet symmetries for SCF, one-state CI, and 28-state calculations. In this figure, we have shown the elastic cross section calculated by including only the ground state which is correlated, where the active space spans orbitals up to 9σ and 3π.

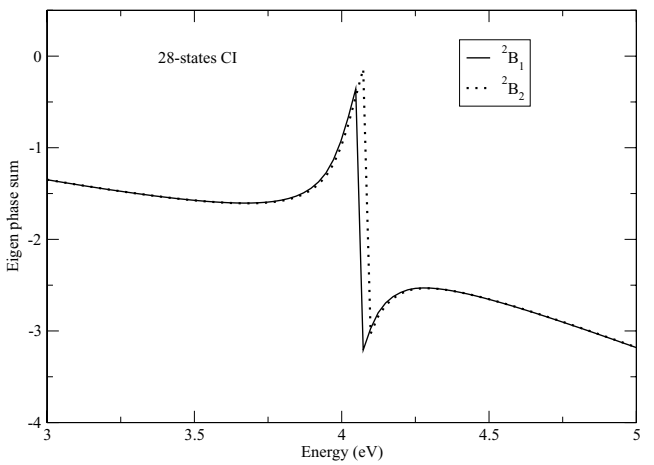

FIG. 4. Eigenphase sum of $^2B_1$ and $^2B_2$ symmetries for 28-state CI calculation. Solid curve, $^2B_1$; dotted curve, $^2B_2$.

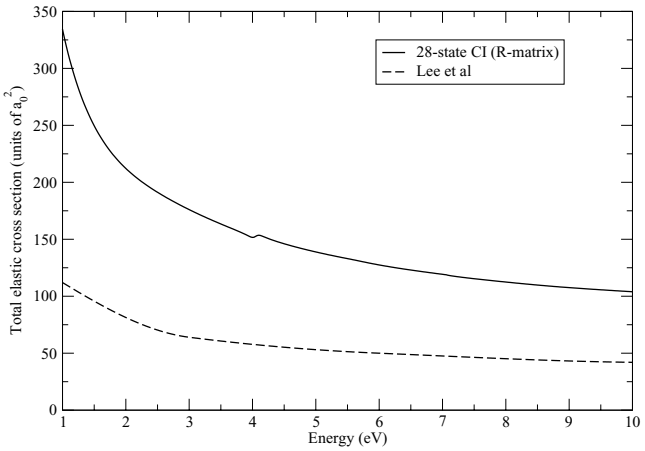

FIG. 5. Comparison of total elastic cross sections (TCSs). Dashed curve, Lee *et al.* [10]; solid curve, *R*-matrix results for 28-state CI calculation.

We notice one peak in the cross sections at 0.77 eV in the SCF calculation and which is shifted to 0.25 eV in the one-state calculation due to inclusion of extra correlation effects. The eigenphase sum shows a sudden jump of π radian centered at this position. This resonance belongs to degenerate $(^2B_1/^2B_2)^2\Pi$ symmetry. To investigate whether this resonance is real, we performed the calculation in a 28-state model. The resonance seen in the SCF and one-state CI model is washed out in this 28-state model due to the inclusion of higher excited states.

The retention of a large number of closed electronic excitation channels in the 28-state model provides the necessary polarization potential in an *ab initio* way; this polarization potential is critical in determining the resonance parameters of the detected resonances. In Fig. 3, we have present the elastic cross sections of the electron impact on the SO molecule at R_e for the 28-state calculation. We have shown the contribution of doublet and quartet symmetries separately. We notice one peak in the cross sections of doublets around 4 eV which is due to degenerate $(^2B_1/^2B_2)^2\Pi$ symmetry. The eigenphase sum shows a sudden jump of π radian centered at this position. The Born correction shown in Fig. 3 is added to the sum of doublets and quartets to get an elastic cross section that includes the contribution of higher partial waves neglected in the *R*-matrix calculation. In Fig. 4, we show the eigenphase sum of $^2B_1$ and $^2B_2$ symmetries in the 28-state model. Figure 5 shows the comparison of total elastic cross sections (TCSs) for the 28-state CI calculation with the calculation of Lee *et al.* [10], who applied the Born-closure approximation at the amplitude level to account for the contribution of the high angular momentum state. We observe that at all values of electron-impact energies, our values lie higher than those of Lee *et al.* [10].

In Figs. 6–8, we show the inelastic cross sections from the ground state to the four physical states whose vertical excitation thresholds along with their dipole moments and the number of CSFs included in the CI expansion are given in Table II.

In Fig. 6 we notice sharp peaks at 4.06 eV, having widths of 0.170 and 0.164 eV in the cross sections of the $X\,^3\Sigma^- – a\,^1\Delta$ and $X\,^3\Sigma^- – b\,^1\Sigma^+$ transitions, respectively. These resonances belong to degenerate $(^2B_1/^2B_2)^2\Pi$ symmetries. We assign a common configuration $2\pi^4 3\pi^2 3\pi$ to these core excited shape resonances which decay to different parent states $a\,^1\Delta$ and $b\,^1\Sigma^+$, respectively, by dissociating a 3π molecular orbital. The resonance properties of these peaks are also given in Table III. We have also shown the electronic excitation results for e-O_2 scattering using the *R*-matrix method [30]. In contrast to the O_2 results for both the excitation processes, there is a marked resonance structure in the case of SO around 4 eV. In general, the cross sections for SO are slightly larger because SO is a bigger molecule than O_2.

Figure 7 depicts the excitation cross section for the optically allowed transition $X\,^3A_2(X\,^3\Sigma^-) – b\,^3A_2(b\,^3\Sigma^-)$. The contribution of quartet and doublet symmetries is shown separately. The contribution of quartets is more than that of doublet symmetries due to their higher spin multiplicity by a factor of nearly 2 than that of doublet symmetries. The Born correction is also included for this dipole transition.

Figure 8 depicts the excitation cross section for the optically allowed transition $X\,^3A_2(X\,^3\Sigma^-) – C^3B_1/^3B_2(C\,^3\Pi)$. The contribution of quartet and doublet symmetries is shown separately. The contribution of quartets is once again higher

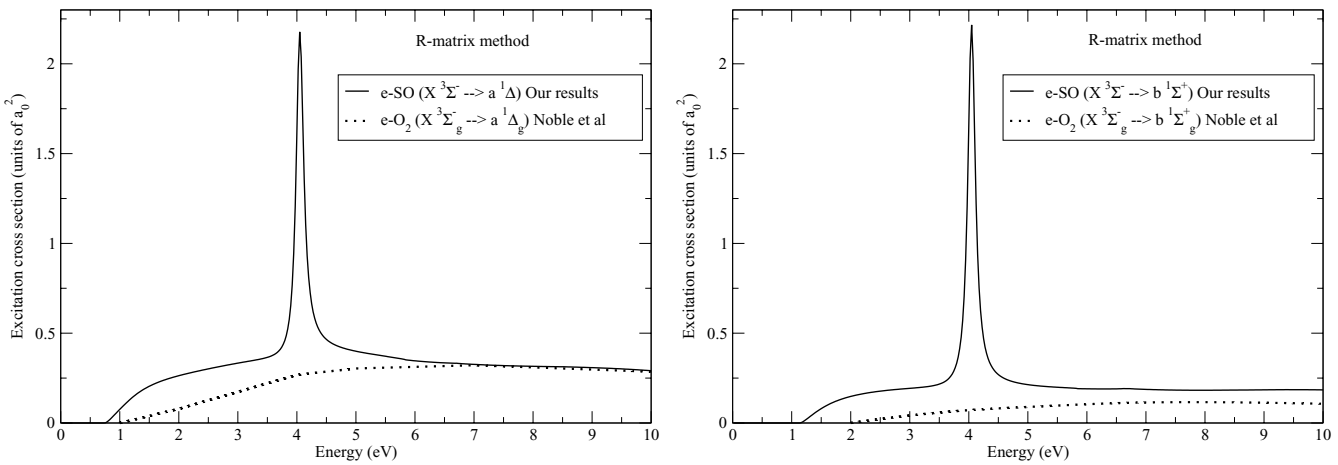

FIG. 6. Electron-impact excitation cross sections from the ground state: $X\,^3\Sigma^-$ ($^3A_2$) of the SO molecule to the $a\,^1\Delta$ $a(^1A_2/^1A_1)$ and $b\,^1\Sigma^+$ $b(^1A_1)$, solid line; $X\,^3\Sigma_g^-$ of the O_2 molecule to the $a\,^1\Delta_g$ and $b\,^1\Sigma_g^+$, dotted curve, from Noble and Burke [30].

TABLE III. Resonance properties of SO at bond length $R = 2.9\ a_0$.

Electronic configuration of resonant state	E_r (eV)	Γ_r (eV)	Type of resonance	Parent state
$1\sigma^2$-$7\sigma^2\ 1\pi^4\ 2\pi^4\ 3\pi^2\ (a\,^1\Delta)(3\pi)\,:\,^2\Pi$	4.06	0.170	Core-excited shape	$a\,^1A_1/^1A_2\ (a\,^1\Delta)$
$1\sigma^2$-$7\sigma^2\ 1\pi^4\ 2\pi^4\ 3\pi^2\ (b\,^1\Sigma^+)(3\pi)\,:\,^2\Pi$	4.06	0.164	Core-excited shape	$b\,^1A_1\ (b\,^1\Sigma^+)$

than that of doublet symmetries. The Born correction is also included for this dipole transition.

B. Ionization cross section

Figure 9 shows electron-impact ionization cross sections of SO from threshold 11.12 eV to 5000 eV by using the standard formalism of the binary-encounter-Bethe (BEB) model [14,15]. This formalism requires the binding energy and kinetic energy of each occupied orbital in a molecular structure calculation. The ionization cross section rises from threshold to a peak value of 4.8 Å^2 at 77.8 eV and then shows $\ln(E/E)$ behavior as E approaches higher values. We have also shown the results of previous theoretical work [8–10]. The molecular orbital data used in the calculation of the BEB cross section is given in Table IV, which is generated at SCF level. The BEB ionization cross section σ is obtained by summing over each orbital cross section σ_i, where

$$\sigma_i(t) = \frac{s}{t+u+1}\left[\frac{1}{2}\left(1-\frac{1}{t^2}\right)\ln t + \left(1-\frac{1}{t}\right) - \frac{\ln t}{t+1}\right], \tag{2}$$

where $t = T/B$, $u = U/B$, and $s = 4\pi {a_0}^2 N(R/B)^2$. Here, R is the Rydberg energy, T is the kinetic energy of the incident electron, U is the orbital kinetic energy, N is the electron occupation number, and B is the binding energy of the orbital.

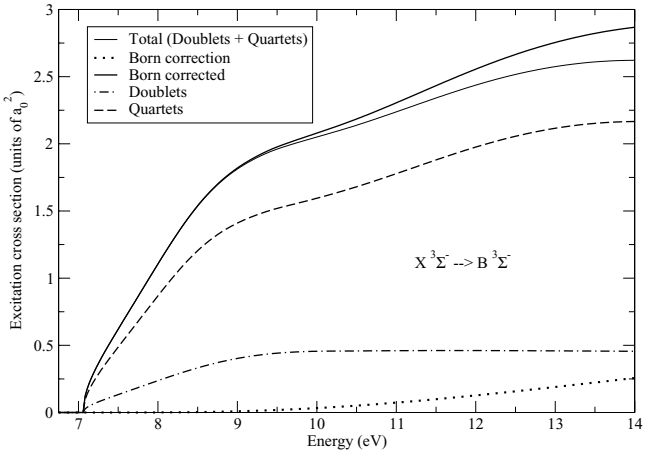

FIG. 7. Electron-impact excitation cross sections from the ground $X\,^3\Sigma^-$ ($^3A_2$) state of the SO molecule to the $b\,^3\Sigma^-$ ($^3A_2$) state for the 28-state calculation. Dash dot curve, doublets sum; dashed curve, quartets sum; thin solid line, total (doublets + quartets); dotted curve, Born correction; thick solid line, Born corrected (sum of doublets, quartets, and Born correction).

C. Differential cross section

The evaluation of the differential cross sections (DCSs) provides a more stringent test for any theoretical model. The rotational excitation cross sections for electron impact on a neutral molecule can be calculated from the scattering parameters of elastic scattering in the fixed nuclei approximation provided the nuclei are assumed to be of infinite masses [31]. In particular, starting from an initial rotor state $J = 0$, the sum of all transitions from the $J = 0$ level to a high enough J value for convergence is equivalent to the elastic cross section in the fixed nuclei approach. We have employed this methodology to extract rotationally elastic and rotationally inelastic cross sections from the K-matrix elements calculated in the one-state R-matrix model. The DCS for a general polyatomic molecule is given by the familiar expression

$$\frac{d\sigma}{d\Omega} = \sum_L A_L P_L(\cos\theta). \tag{3}$$

where P_L is a Legendre polynomial of order L. The A_L coefficients have already been discussed in detail [32]. For a polar molecule, this expansion over L converges slowly. To circumvent this problem, we use the closure formula

$$\frac{d\sigma}{d\Omega} = \frac{d\sigma^B}{d\Omega} + \sum_L \left(A_L - {A_L}^B\right) P_L(\cos\theta). \tag{4}$$

The superscript B denotes that the relevant quantity is calculated in the Born approximation with an electron-point dipole interaction. The convergence of the series is now rapid, since the contribution from the higher partial waves to the DCS is dominated by the electron-dipole interaction. The quantity $\frac{d\sigma}{d\Omega}$ for any initial rotor state $|Jm\rangle$ is given by the sum over all

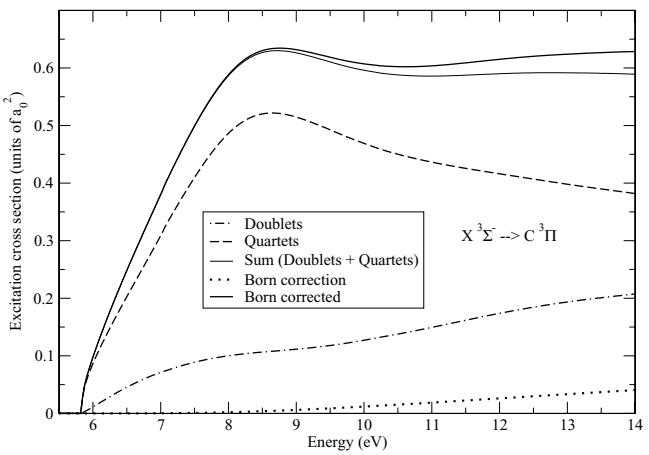

FIG. 8. Same as Fig. 7, but for the ground $X\,^3\Sigma^-$ ($^3A_2$) state of the SO molecule to the $C^3\Pi$ ($^3B_1/^3B_2$) state for the 28-state calculation.

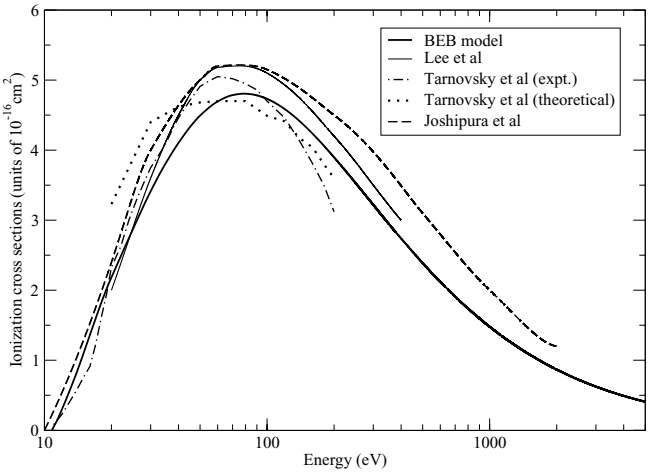

FIG. 9. Electron-impact BEB ionization cross sections of the SO molecule. Dashed curve, Joshipura *et al.* [9]; dotted curve, Tarnovsky *et al.* (theor.) [8]; dash-dot curve, Tarnovsky *et al.* (expt.) [8]; thin solid curve, Lee *et al.* [10]; thick solid line, our BEB model.

final rotor states $|J'm'\rangle$

$$\frac{d\sigma}{d\Omega} = \sum_{J'm'} \frac{d\sigma}{d\Omega}(Jm \to J'm'). \tag{5}$$

where J is the rotational angular momentum, and m is its projection on the internuclear axis. To obtain converged results, the maximum value of $J' = 5$ and $L = 30$. We have calculated DCS by using the POLYDCS program of Sanna and Gianturco [33], which requires basic molecular input parameters along with K matrices evaluated in a particular scattering calculation. We have used this code to compute the DCS in the one-state CI model. Since SO is an open-shell molecule having $X\,^3\Sigma^-$ as its ground state, the spin coupling between this target state and the spin of the incoming electron allows two spin-specific channels, namely, the doublets (D) and quartets (Q) couplings. The spin-averaged DCS for elastic electron scattering from the SO radical are calculated by using the statistical weight 2/6 for doublet and 4/6 for quartet scattering channels. We then

TABLE IV. SO molecular orbital binding and average kinetic energies for the DZ+P basis set at equilibrium geometry. $|B|$ is binding energy (eV), U is kinetic energy (eV), and N is occupation number.

Molecular orbital	$\|B\|$ (eV)	U (eV)	N
$1\sigma(1a_1)$	2505.28	3296.87	2
$2\sigma(2a_1)$	560.84	794.53	2
$3\sigma(3a_1)$	246.64	509.37	2
$4\sigma(4a_1)$	183.48	478.62	2
$1\pi(1b_1)$	183.42	478.62	2
$1\pi(1b_2)$	183.42	478.08	2
$5\sigma(5a_1)$	38.34	77.00	2
$6\sigma(6a_1)$	23.73	75.64	2
$7\sigma(7a_1)$	16.45	66.39	2
$2\pi(2b_1)$	15.81	61.22	2
$2\pi(2b_2)$	15.81	61.22	2
$3\pi(3b_1)$	5.56	54.42	1
$3\pi(3b_1)$	5.56	54.42	1

TABLE V. Number of coupled channels for a doublet or a quartet scattering symmetry of SO molecule for 28-state calculation.

Scattering symmetry	Number of coupled channels
$^2A_1$	174
$^2B_1$	176
$^2B_2$	176
$^2A_2$	174
$^4A_1$	90
$^4B_1$	95
$^4B_2$	95
$^4A_2$	95

use Eq. (3) as follows to calculate the DCS:

$$\frac{d\sigma}{d\Omega} = \frac{1}{3}\left[2\left(\frac{d\sigma}{d\Omega}\right)^Q + \left(\frac{d\sigma}{d\Omega}\right)^D\right], \tag{6}$$

where $(\frac{d\sigma}{d\Omega})^{Q,D}$ represent DCS for quartet and doublet cases, respectively. [The number of coupled channels for a doublet or a quartet scattering symmetry are shown later in Table V.] The number of closed channels depend upon the scattering energy of the incident electron.

In Fig. 10, we show the spin-averaged DCSs calculated in the one-state R-matrix model at different energies. We have compared our results with results of Lee *et al.* [10], who used the iterative Schwinger variational method at the static-exchange-polarization absorption level. At 2 eV, as we approach forward angles, the DCSs rise abruptly due to the dipolar nature of the SO molecule. Our results are in reasonable agreement with the results of Lee *et al.* [10] for angles up to 40°, beyond which our results are slightly lower, this is due to large correlation effects included in the CI model in the present calculations. We notice similar trends at 4, 6, 8, and 10 eV, which are shown in Fig. 10.

Besides this, the data on DCS are further used to calculate the momentum-transfer cross section (MTCSs), which show the importance of backward angle scattering. Since the DCSs are not very sensitive to correlation effects for backward scattering, we expect our MTCSs to be quite reliable in the 0.01–10 eV range. These are calculated in the one-state CI model with spin averaging. MTCS provides a useful input in solving the Boltzmann equation for the electron distribution function. In contrast to the diverging nature of DCS in the forward direction, MTCS shows no singularity due to the weighting factor $(1 - \cos\theta)$, where θ is the scattering angle. This factor vanishes as $\theta \to 0$. The MTCS is useful in the study of electrons drifting through a molecular gas. When a swarm of electrons travel through a molecular gas under the influence of an electric field, several transport observables such as diffusion coefficient D and mobility μ can be obtained if we have a knowledge of the momentum-transfer cross sections. In Fig. 11, we show the comparison of calculated MTCSs with those of [10]. We observe that at high energy, they both seem to be converging.

D. Effective collision frequency of electrons

The effective electron-neutral collision frequency $\langle v\rangle$ which is averaged over a Maxwellian distribution can be obtained

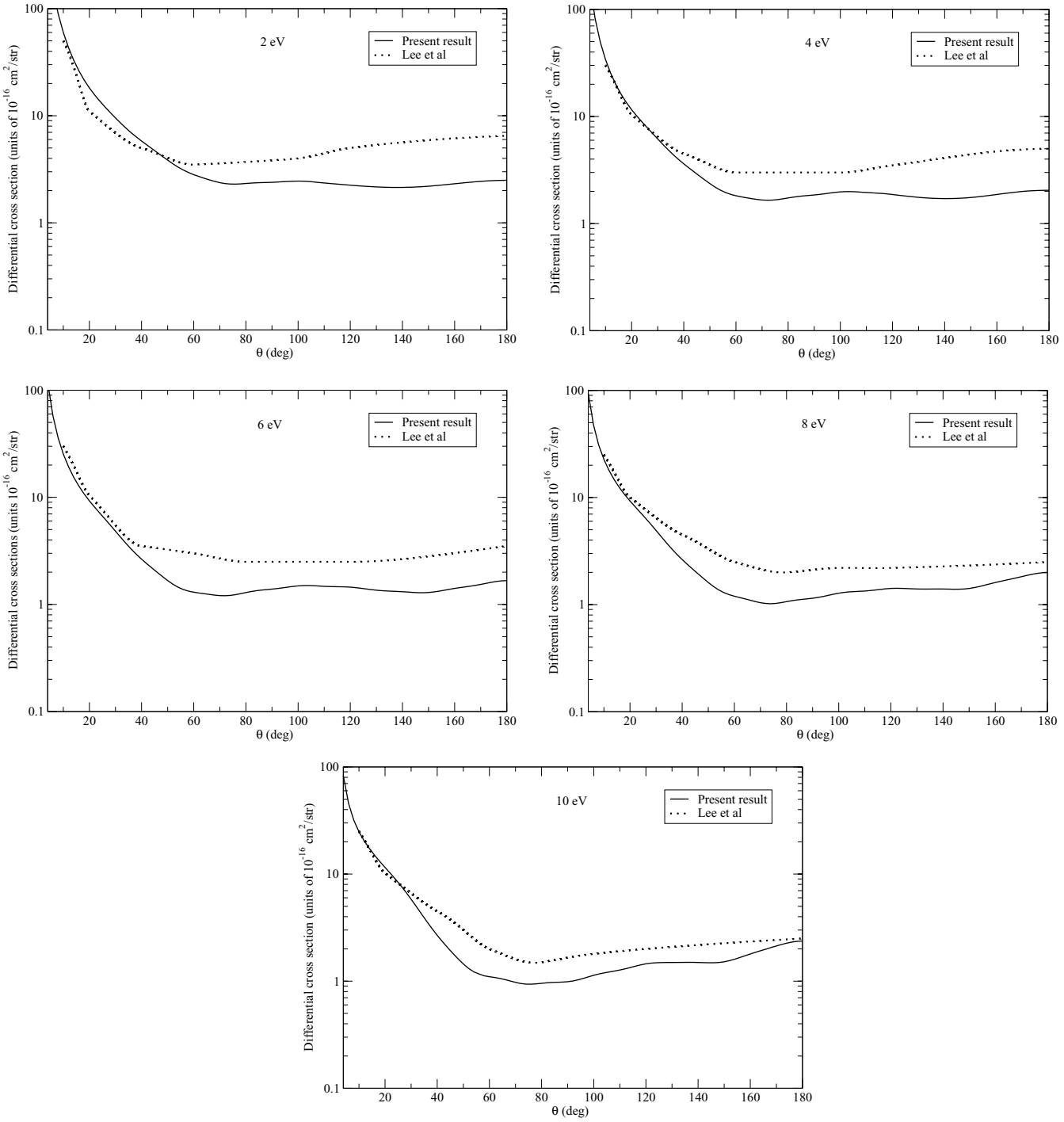

FIG. 10. Comparison of differential cross sections (DCSs) at 2, 4, 6, 8, and 10 eV. Dotted curve, Lee *et al.* [10]; solid curve, present result (with spin-average) for one-state CI model at R_e.

from the momentum-transfer cross section $Q^{(m)}(v)$ as follows [34]:

$$\langle v\rangle = \frac{8}{3\pi^{1/2}} N \left(\frac{m_e}{2kT_e}\right)^{5/2} \int_0^\infty v^5 Q^{(m)}(v) \exp\left(\frac{-m_e v^2}{2kT_e}\right) dv, \tag{7}$$

where m_e and T_e are the electron mass and temperature, respectively, k is Boltzmann's constant, v is the velocity, and N is the number density of the gas particles. The averaging is over a Maxwellian speed distribution function for an electron temperature T_e which is given by

$$f(v) = 4\pi v^2 \left(\frac{m_e}{2\pi kT_e}\right)^{3/2} \exp\left(\frac{-m_e v^2}{2kT_e}\right). \tag{8}$$

This type of collision frequency is often used to evaluate the energy transfer between particles. Alternatively, the effective

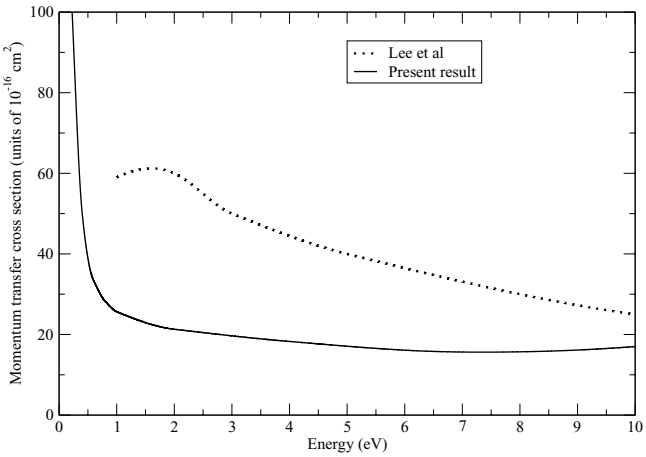

FIG. 11. Momentum-transfer cross sections (MTCSs) at different energies. Dotted curve, Lee *et al.* [10]; solid curve, with spin average of the SO molecule ground state at the one-state CI level.

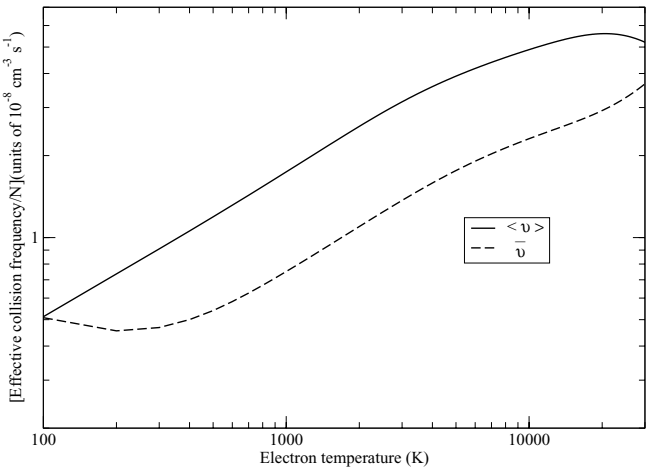

FIG. 12. Effective collision frequency as a function of electron temperature. Dashed curve, $\bar{\upsilon}$; solid curve, $\langle \upsilon \rangle$.

collision frequency for electrons can be defined from the dc conductivity as follows [34,35]:

$$\bar{\upsilon}^{-1} = \frac{8}{3\pi^{1/2}N}\left(\frac{m_e}{2kT_e}\right)^{5/2}\int_0^\infty \frac{v^3}{Q^{(m)}(v)}\exp\left(\frac{-m_e v^2}{2kT_e}\right)dv. \tag{9}$$

This explicit form of effective collision frequency $\bar{\upsilon}$ is related to the drift velocity of electrons in a gas, insofar as a Maxwell distribution can be assumed. When $Q^{(m)}(v)$ is proportional to v^{-1}, the two effective collision frequencies $\langle \upsilon \rangle$ and $\bar{\upsilon}$ agree. Figure 12 shows both types of effective collision frequencies as a function of electron temperature. Note that $\langle \upsilon \rangle$ lies higher than $\bar{\upsilon}$ in the entire electron temperature range.

IV. CONCLUSIONS

This is a comprehensive *ab initio* study of electron impact on the SO molecule using the UK molecular *R*-matrix codes. Elastic (integrated and differential), momentum-transfer, excitation, and ionization cross-section have been presented. The results of the SCF, one-state CI, and 28-state close-coupling approximation are presented. We detect a stable bound state of SO^- having the configuration $1\sigma^2 2\sigma^2 3\sigma^2 4\sigma^2 1\pi^4 5\sigma^2 6\sigma^2 7\sigma^2 2\pi^4 3\pi^3$ with a vertical electronic affinity value of 0.970 eV, which is in good agreement with the estimated experimental value of about 1.125 eV. The target states are represented by including correlations via a configuration-interaction technique. Our target calculations give reasonable agreement with the calculated vertical excitation spectrum of Borin *et al.* [27]. The derived MTCS from DCS and two types of effective collision frequencies have also been presented that may be useful to the scientific community.

[1] A. L. Broadfoot *et al.*, Science **204**, 979 (1979); **206**, 962 (1979).
[2] K. Becker, W. van Wijngaarden, and J. W. McConkey, Planet. Space Sci. **31**, 197 (1983).
[3] A. S. Hoffman, J. Appl. Polym. Sci.: Appl. Polym. Symp. **42**, 251 (1988).
[4] I. Gallinberti, Pure Appl. Chem. **60**, 663 (1988).
[5] M. B. Chang, M. J. Kushner, and M. J. Rood, Plasma Chem. Plasma Process. **12**, 565 (1992).
[6] B. E. Turner, Astrophys. J. **455**, 556 (1995).
[7] Z. Cao and D. W. Setser, J. Phys. Chem. **92**, 1169 (1988).
[8] V. Tarnovsky, A. Levin, H. Deutsch, and K. Becker, J. Chem. Phys. **102**, 770 (1995).
[9] K. N. Joshipura and S. Gangopadhyay, J. Phys. B **41**, 215205 (2008).
[10] M.-T. Lee, I. Iga, L. E. Machado, and L. M. Brescansin, Phys. Rev. A **80**, 022706 (2009).
[11] L. A. Morgan, C. J. Gillan, J. Tennyson, and X. Chen, J. Phys. B **30**, 4087 (1997).
[12] L. A. Morgan, J. Tennyson, and C. J. Gillan, Comput. Phys. Commun. **114**, 120 (1998).
[13] J. Tennyson, J. Phys. B **29**, 1817 (1996).
[14] Y. K. Kim and M. E. Rudd, Phys. Rev. A **50**, 3954 (1994).
[15] W. Hwang, Y. K. Kim, and M. E. Rudd, J. Chem. Phys. **104**, 2956 (1996).
[16] C. W. McCurdy and T. N. Rescigno, Phys. Rev. A **39**, 4487 (1989).
[17] P. G. Burke and K. A. Berrington *Atomic and Molecular Processes: An R-matrix Approach* (IOP Publishing, Bristol, UK, 1993).
[18] C. J. Gillan, J. Tennyson, and P. G. Burke, in *Computational Methods for Electron-Molecule Collisions*, edited by W. M. Huo and F. A. Gianturco (Plenum, New York, 1995).
[19] K. L. Baluja, P. G. Burke, and L. A. Morgan, Comput. Phys. Commun. **27**, 299 (1982).
[20] L. A. Morgan, Comput. Phys. Commun. **31**, 419 (1984).
[21] B. M. Nestmann, K. Pfingst, and S. D. Peyerimhoff, J. Phys. B **27**, 2297 (1994).
[22] J. Tennyson, J. Phys. B **29**, 6185 (1996).
[23] A. Faure, J. D. Gorfinkiel, L. A. Morgan, and J. Tennyson, Comput. Phys. Commun. **144**, 224 (2002).

[24] T. H. Dunning and P. J. Hay, in *Methods of Electronic Structure Theory*, Vol. 2, edited by H. F. Schaefer (Plenum, New York, 1977).
[25] [http://cccbdb.nist.gov/].
[26] W. C. Swope, Y.-P. Lee, and H. F. Schaefer III, J. Chem. Phys. **71**, 3761 (1979).
[27] A. C. Borin and F. R. Ornellas, Chem. Phys. **247**, 351 (1999).
[28] S. Kaur, K. L. Baluja, and J. Tennyson, Phys. Rev. A **77**, 032718 (2008).
[29] M. T. N. Varella, M. H. F. Bettega, M. A. P. Lima, and L. G. Ferreira, J. Chem. Phys. **111**, 6396 (1999).
[30] C. J. Noble and P. G. Burke, J. Phys. B **19**, L35 (1986).
[31] E. S. Chang and A. Temkin, Phys. Rev. Lett. **23**, 399 (1969).
[32] F. A. Gainturco and A. Jain, Phys. Rep. **143**, 347 (1986).
[33] N. Sanna and F. A. Gianturco, Comput. Phys. Commun. **114**, 142 (1998).
[34] Y. Itikawa, Phys. Fluids **16**, 831 (1973).
[35] I. P. Shkarofsky, Can. J. Phys. **39**, 1619 (1961).